Mechanism of the Verwey transition in magnetite: Jahn–Teller distortion and charge ordering patterns

2006 J. Phys.: Condens. Matter 18 10427

(http://iopscience.iop.org/0953-8984/18/46/010)

INSTITUTE OF PHYSICS PUBLISHING JOURNAL OF PHYSICS: CONDENSED MATTER

J. Phys.: Condens. Matter **18** (2006) 10427–10436 doi:10.1088/0953-8984/18/46/010

Mechanism of the Verwey transition in magnetite: Jahn–Teller distortion and charge ordering patterns

H P Pinto and S D Elliott

Tyndall National Institute, Lee Maltings, Cork, Republic of Ireland

E-mail: hpp@fyslab.hut.fi and simon.elliott@tyndall.ie

Received 1 September 2006, in final form 29 September 2006
Published 3 November 2006
Online at stacks.iop.org/JPhysCM/18/10427

Abstract

We have performed density functional calculations with on-site Coulomb repulsion corrections of systems that may be involved in the Verwey transition in magnetite (Fe_3O_4). We find that the lowest energy solution for the minority spin wavefunction in the cubic cell involves orbitally ordered Fe-d and O-p states, which breaks cubic symmetry. This leads to partial charge ordering that triggers a Jahn–Teller distortion and band-gap opening. Our results show this to be the essential mechanism of the Verwey transition. Applying ionic relaxation within a larger tetragonal cell, three patterns of charge ordering are compared and a *Pmca* pattern matching x-ray data is found to be the most stable.

M Supplementary data files are available from stacks.iop.org/JPhysCM/18/10427

1. Introduction

Magnetite Fe_3O_4 is a fascinating material that is still not well understood and presents challenges for state-of-the-art computational methods. This transition metal oxide with strongly correlated electrons is a typical Neél ferrimagnet ($T_N = 858$ K) and a promising material for spintronic applications [1]. Magnetite undergoes a Verwey transition [2] at $T_V = 121$ K where the high-temperature spinel structure ($Fd\bar{3}m$) lowers its symmetry to monoclinic Cc [3, 4]. During this metal–insulator transition (MIT), the resistivity drops by two orders of magnitude with fundamental changes of its electronic structure. A band-gap opening is observed: photoemission spectroscopy [5, 6] and optical conductivity [7] experiments clearly show a band gap of ∼0.14 eV below T_V.

To explain this, Verwey proposed a simple charge ordering (CO) of alternating strips of Fe_B^{3+} and Fe_B^{2+} along [1 1 0] and [$\bar{1}$ 1 0] directions respectively (A and B denote the tetrahedral and octahedral sites), but this model is too simple in a number of respects. Firstly, the ions in complex oxides do not show integer charges that match formal oxidation states [8]. Furthermore, whether non-integer CO is present in Fe_3O_4 is still under active discussion [9, 10].

Experimental studies including magnetic after-effect [9], x-ray diffraction [4], resonant x-ray diffraction [11, 12], electron diffraction [13] and high-energy electron transmission [14] support some level of CO in Fe_3O_4. But, on the other hand, neutron diffuse scattering [15] and x-ray resonant scattering [16] suggest an itinerant picture for B-site electrons. Our aim is to determine whether CO is energetically favourable at low temperature and whether this is a sufficient condition for the band-gap opening. To do this, we study the 14-atom cubic primitive cell (pc), which contains two inequivalent Fe_B in one Fe_4O_4 minicube. The symmetry of the pattern of CO proposed by Verwey is also inconsistent with experiment. To investigate more realistic CO patterns, we relax fully the atomic coordinates of a 56-atom tetragonal $a/\sqrt{2} \times a/\sqrt{2} \times 2a$ cell, both within *Pmca* [4] and lower symmetry.

Uncertainty also remains about the structure of the low-temperature Cc phase, due to experimental difficulties. By fitting to x-ray data, Iizumi *et al* [3] and later Wright *et al* [4] have obtained a $P2/C$ monoclinic cell containing 56 atoms in a *Pmca* arrangement (two distinct Fe_A, four distinct Fe_B and two distinct Fe_4O_4 minicubes per cell). This has been confirmed by resonant x-ray diffraction [11, 12]. There is only one *Pmca* CO pattern that divides the Fe_B into two equal groups and so it is no surprise that theoretical studies at this geometry (without relaxation) using local density approximation with on-site Coulomb corrections (LDA $+$ U) [17, 18] confirm the experimental pattern of CO modulated along [0 0 1]. These calculations also reveal the associated orbital ordering (OO) pattern. However these calculations do not clarify what factors drive the band-gap opening—suggestions include Fe_B–Fe_B interaction [19], a [0 0 1] charge density wave [4], elastic versus electrostatic factors [17], orbital ordering [18] and long-range ordering of Fe_B–O distortions [20]. We use the models described above to explore these questions.

Our results show a complex MIT that involves not only Fe-d states but also O-p, with symmetry breaking of the wavefunction that triggers a Jahn–Teller (JT) deformation of O about Fe_B and a band-gap opening. CO is frustrated on the cubic Fe_B sublattice [21], so that further deformation and an increase in cell size are associated with the MIT.

2. Method

The calculations have been performed using the plane wave basis Vienna *ab initio* simulation package (VASP) [22, 23], implementing spin-polarized density functional theory (DFT) and the generalized gradient approximation (GGA) [24] with an intra-site Coulomb interaction between Fe-d electrons in Dudarev's approach [25]; we call the method GGA $+ U$.[1] We describe the O–$1s^2$ and Fe–[Ne] core electrons with projector augmented wave (PAW) potentials [26]. Using a kinetic energy cutoff of 400 eV and a dense k-point mesh (we used a 0.03 $Å^{-1}$ k-point separation that corresponds to a $7 \times 7 \times 7$ Monkhorst–Pack (MP) grid for the 14-atom cubic pc, 172 irreducible k-points; $5 \times 5 \times 3$ MP grid for the 56-atom tetragonal cell, 38 irreducible k-points), we converge the total energy to <2 meV/fu (fu $=$ formula unit Fe_3O_4). The ionic optimizations were performed until all the forces were <0.01 eV $Å^{-1}$.

We started computing the physical properties of Fe_3O_4 in the cubic phase using the spin-polarized GGA. The outcome is a ferrimagnetic semi-metallic $Fd\bar{3}m$ crystal with lattice constant $a_{GGA} = 8.373$ Å, magnetic moment $m_{GGA} = 4.0\ \mu_B$/fu and bulk modulus $B_{0-GGA} =$ 1.82 Mbar. These values are in close agreement with experimental ones in the cubic phase:

[1] In Dudarev's approach, the on-site Coulomb interaction energy $E_{\mathcal{U}}$ is $\frac{(\bar{U}-\bar{J})}{2} \sum_\sigma [\mathrm{Tr}(n^\sigma) - \mathrm{Tr}(n^\sigma n^\sigma)]$, where n^σ is the density matrix of the d electrons, σ is a spin index and $\bar{U}$ and $\bar{J}$ are the spherically averaged matrix elements of the screened Coulomb and exchange interactions, respectively. In this approach only the difference $\mathcal{U} = (\bar{U} - \bar{J})$ is meaningful.

$a_{\mathrm{Expt}} = 8.3956$ Å [27], $m_{\mathrm{Expt}} = 4.05\ \mu_{\mathrm{B}}$/fu [28] and $B_{0-\mathrm{Expt}} = 1.81 \pm 0.05$ Mbar [29]. Moreover, the predicted $Fd\bar{3}m$ structure is at the GGA global minimum: we performed a molecular dynamics (MD) simulation, only on the internal coordinates, for about 2 ps at a constant temperature of 120 K with a subsequent ionic relaxation; the GGA result is again the original cubic $Fd\bar{3}m$ structure with a semi-metallic ground state. This means that the GGA is unable to reproduce the minority spin band gap—an important feature of Fe_3O_4 at $T \leqslant T_{\mathrm{V}}$.

The next stage was to apply GGA + U to see if it can reproduce the band-gap opening. We began with the optimized lattice constant from the GGA and assigned a high value of $\mathcal{U} = (\bar{U} - \bar{J}) = 5$ eV for Fe-d electrons at both Fe_A and Fe_B sites. Performing MD on the ions—in the same fashion as before—and including a final relaxation gave a structure with lower energy and lower symmetry ($C2/C$) that showed a band-gap opening.

Based on this result, we proceeded to systematically study the effect of $\mathcal{U}$ on both the electronic and the atomic structures. At each $\mathcal{U}$ value, we optimized the $Fd\bar{3}m$ semi-metallic structure (lattice and ions) and then applied MD with a subsequent relaxation—only on the ions—ending with the analysis of the electronic structure, in particular a possible band-gap opening. The results reveal a range of $\mathcal{U}$ values where the band gap—for the low symmetry solution—is between 0.1 and 0.4 eV. We chose $\mathcal{U}_{\mathrm{op}} = 3.8$ eV that corresponds to a band gap of 0.33 eV.

The first exciting prediction of this method is the existence of at least three different self-consistent solutions for the electronic density within the perfect cubic $Fd\bar{3}m$ structure of Fe_3O_4. In other words, a proper consideration of the intra-site interaction between d electrons gives some 'extra' degrees of freedom to the wavefunction, allowing the system to achieve various OO patterns, or self-consistent states with lower symmetry than that of the confining potential given by the ionic configuration. The lower symmetry OO wavefunction—within the cubic $Fd\bar{3}m$ structure—was obtained by using the wavefunction of the low-symmetry $C2/C$ structure as the initial guess for the calculation of the cubic $Fd\bar{3}m$ system, and then iterating to self-consistency with GGA + U.

Finally, we used GGA + U to relax atomic coordinates within the tetragonal $a/\sqrt{2} \times a/\sqrt{2} \times 2a$ cell (using the GGA + U cubic a parameter), in order to investigate CO patterns. Optimization of the *Pmca* internal coordinates of Wright *et al* [4] produced a minimum-energy structure that preserved *Pmca* symmetry. An alternative structure, with $P1$ symmetry, was obtained by free optimization from a supercell of the $C2/C$ coordinates.

3. Results: structure and electronic properties

3.1. 14-atom cubic model

Using $\mathcal{U}_{\mathrm{op}}$, we once again computed the physical properties of the perfect cubic Fe_3O_4 (E_{C} in figure 1); here the Fe_B–O and Fe_A–O distances are 2.07 and 1.90 Å, respectively. The result for $a_{\mathrm{GGA}+U}$, $m_{\mathrm{GGA}+U}$ and $B_{0-\mathrm{GGA}+U}$ are 8.446 Å, 4.0 μ_{B}/fu and 1.71 Mbar, respectively.

The outcome of MD and subsequent relaxation—only on the internal coordinates—is a structure denoted E_{min} whose atoms exhibit monoclinic $C2/C$ symmetry within the cubic cell, with an energy of 352 meV/fu lower than E_{C} (figure 1). Its minority spin (↓) electronic structure reveals an indirect band gap of 0.33 eV (figure 2(d)). Repeating the ionic relaxation after a different random perturbation yielded an alternative structure, with orthorhombic *IMMA* symmetry and an energy 348 meV/fu lower than E_{C}. In both $C2/C$ and *IMMA* relaxed structures there was imperceptible distortion of the Fe_B ions. Meanwhile, the mean displacements ($\overline{\Delta r}$) for Fe_A and O ions of $C2/C$ (*IMMA*) structure are $\overline{\Delta r}(\mathrm{Fe_A}) = 0.04$ (0.04) Å and $\overline{\Delta r}(\mathrm{O}) = 0.07$ (0.06) Å relative to $Fd\bar{3}m$. Because both low-symmetry structures show similar electronic structure, we chose the $C2/C$ structure for further study.

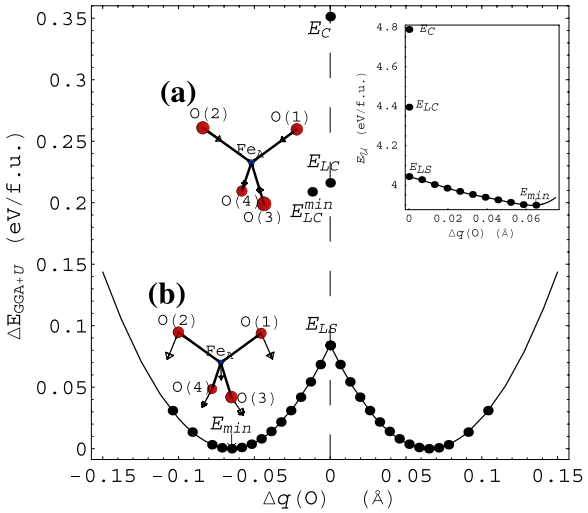

Figure 1. Frozen phonon calculation of energy versus O displacements (Δq(O)). At Δq(O) = 0 Å ($Fd\bar{3}m$ structure) there are three different self-consistent GGA + U solutions $E_{\rm C}$ (315 meV), $E_{\rm LC}$ (216 meV) and $E_{\rm LS}$ (84 meV). (a) Distortion of the O ions (magnified 50 times) around Fe_A for $E_{\rm LC}^{\rm min}$ (208 meV). (b) Distortion of the O ions (magnified 18 times) around Fe_A for $E_{\rm min}$ (0 meV); the tiny displacement of Fe_A defines the preferential axis. The inset shows the variation of the E_{U} contribution to the total energy versus displacement Δq(O).

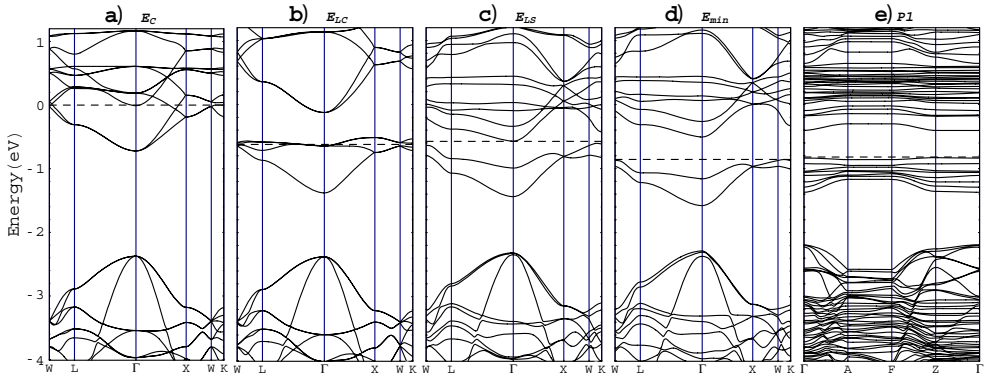

Figure 2. The computed GGA + U minority spin ↓ band structure within the cubic model along the high-symmetry points (W, L, Γ, X and K) of the reciprocal cubic cell of: (a) $E_{\rm C}$, (b) $E_{\rm LC}$, (c) $E_{\rm LS}$ and (d) $E_{\rm min}$ states, corresponding to figure 1. Also shown is the ↓ band structure of tetragonal $P1$ (e). All the bands were shifted to match the O-2s states (−19 to −20.3 eV and not shown here) with those of $E_{\rm C}$. The dashed line denotes $E_{\rm F}$.

In figure 1 we present a frozen phonon calculation of energy versus ionic displacements (Δq). At $\Delta q = 0$ Å (perfect $Fd\bar{3}m$ structure), we found three different self-consistent GGA + U solutions namely: $E_{\rm C}$, $E_{\rm LC}$ and $E_{\rm LS}$ (figure 1). The highest solution for cubic symmetry, $E_{\rm C}$, is metastable at $\Delta q = 0$ and its majority spin (↑) electronic structure (not illustrated) has a band gap of ∼1.7 eV. The Fermi level ($E_{\rm F}$) lies in the minority spin (↓) sub-band (width ∼1.9 eV, figure 2(a)) occupied by two electrons per pc (figure 3(a)). These are delocalized over all Fe_B sites with predominantly $3d(t_{2g})$ character and tiny O-2p contribution. The magnetic moment on Fe_B-sites is 3.93 $\mu_{\rm B}$.

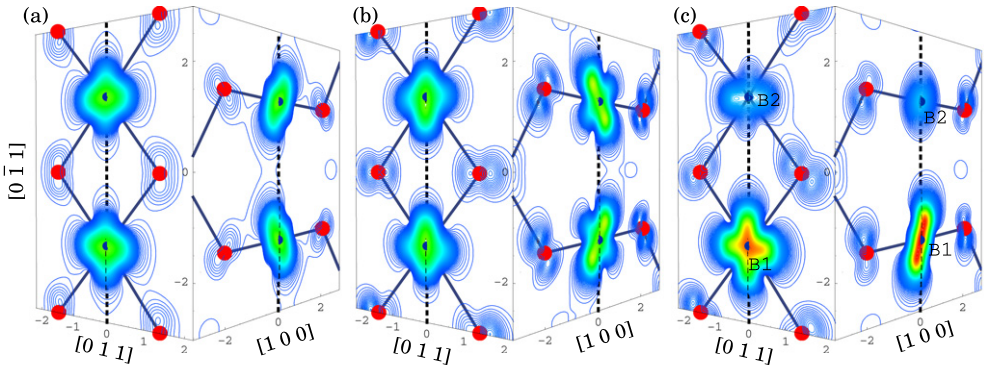

Figure 3. Charge density plots on the (1 0 0) and (0 $\bar{1}$ 1) planes for the two $\downarrow$ electrons within the cubic pc occupying the sub-band just below E_F in figure 2 for (a) E_C, (b) E_{LC}, (c) $E_{LS} = E_{min}$. The two planes intersect at the dotted vertical line which joins Fe_B (blue) and not at the corner as shown and the O atoms are the red points.

The unstable solution E_{LC} (at 216 meV/fu in figure 1) has a wavefunction with cubic symmetry and relaxes, preserving the $Fd\bar{3}m$ symmetry, to the metastable state E_{LC}^{min} at 208 meV/fu (figure 1). This energy lowering involves only symmetrical inward displacements of O atoms ($\Delta q(O) \simeq 0.012$ Å) around Fe_A. The electronic structure of E_{LC} is similar to that of E_{LC}^{min}: both present a drop of E_F by ∼0.6 eV relative to E_C with the formation of a sub-band (0.86 eV wide) that crosses E_F, and a ∼0.38 eV gap separating the empty conduction band levels (figure 2(b)). In this sub-band there are two electrons delocalized on the four Fe_B sites of the pc with appreciable charge transfer to the O-2p states relative to E_C. The occupancies of Fe_B-d orbitals show directional OO pointing to the centre of the Fe_4O_4 minicube, and the O-2p states present a depletion towards the centre of the same minicube (figure 3(b)). This solution has not been reported in some studies of Fe_3O_4 using similar methods [30–34] but is similar to Fe_{B1} in [17]. Certainly the d–d short-range (on-site) Coulomb interactions lead to the drop of E_F, reflecting increased effective screening between the two electrons. The magnetic moment on the Fe_B-sites is 3.90 μ_B, similar to E_C.

The lowest energy solution that we find at $\Delta q = 0$ is denoted E_{LS} and relaxes to the $C2/C$ structure (E_{min}, figure 1). E_{LS} has a broken symmetry wavefunction at $\Delta q = 0$, with a new sub-band ∼0.87 eV wide just below E_F (figure 2(c)). The valence bands do not cross E_F but the band gap between the top of the conduction band at Γ and a point that is the bottom of the conduction band, near K, is negligible, i.e. the system has become an indirect semiconductor with no band gap (at this unstable geometry). Here, the two electrons show a partial CO state in alternating (0 0 1) planes (figure 3(c)). Looking at the occupation matrices, we see a large increase on two of the four Fe_B-sites (B1) to 0.8, with mainly d_{yz} character. Accompanying this, the magnetic moment on Fe_{B1} decreases to 3.63 μ_B. The occupancies of the two remaining Fe_B (B2) decrease to 0.3, which is a mixture of all Fe-d that hybridizes to O-2p (figure 3(c)), and the Fe_{B2} magnetic moment increases to 4.10 μ_B.

The unstable state E_{LS} undergoes a distortion of O ($\Delta q(O) \simeq 0.07$ Å) and Fe_A ($\Delta q(Fe_A) \simeq 0.04$ Å) atoms from cubic $Fd\bar{3}m$ symmetry to $C2/C$, to give E_{min} (figure 1). The Fe_{B1}–O (Fe_{B2}–O) mean distances increase (decrease) to 2.12 (2.05) Å in the y–z plane and 2.06 (2.05) Å along the x direction (see table 1). This opens a spin $\downarrow$ band gap in E_{min} (figure 2(d)). The occupancies and the character of the d electrons and the local magnetic moments show almost no changes across the frozen phonon from E_{LS} to E_{min}. The sub-band just below E_F

Table 1. Fe_B–O distances (d, Å) and average distance to O at each Fe_B site ($\bar{d}$, Å) computed with GGA + U for Fe_3O_4; relative energetics are also given. We assign Fe_B with computed $\bar{d} > 2.07$ Å as Fe_{B1} with partial localization of an extra ↓ electron (formally Fe^{2+}); shorter $\bar{d} < 2.07$ Å indicate Fe_{B2} (Fe^{3+}). The experimental structure, with Fe_B labelled B1, B2, B3, B4 within *Pmca*, is from [4].

Cubic	Cubic		Tetragonal	Tetragonal		Monoclinic	
$Fd\bar{3}m$	$C2/C$, E_{min}		$P1$	*Pmca*		expt *Pmca*	
d	$\bar{d}$	d	$\bar{d}$	$\bar{d}$	d	$\bar{d}$	d
2.068 × 6	B1: 2.103	2.132 × 2	2.112	2.111	2.140 × 2	B1: 2.072	2.091 × 2
		2.112 × 2	2.111		2.140		2.091
		2.064 × 2	2.110		2.136 × 2		2.082 × 2
			2.108		2.057 × 2		2.042 × 2
			2.107	2.108	2.134 × 2	B4: 2.069	2.094 × 2
			2.106		2.111		2.086
			2.104		2.109 × 2		2.053 × 2
			2.100		2.053		2.033
	B2: 2.041	2.052 × 2	2.052	2.033	2.046 × 2	B2: 2.043	2.052 × 2
		2.046 × 2	2.043		2.037 × 2		2.040 × 2
		2.025 × 2	2.042		2.014 × 2		2.038 × 2
			2.040	2.045	2.121	B3: 2.050	2.116
			2.036		2.080 × 2		2.092 × 2
			2.035		2.004 × 2		2.018 × 2
			2.033		1.981		1.964
			2.028				
$\Delta E = +0.352$ eV/fu	$\Delta E = 0$ eV/fu		$\Delta E = -0.010$ eV/fu	$\Delta E = -0.026$ eV/fu			

is ∼0.7 eV wide and it is likely that Fe_{B2}–O overlap is responsible for the dispersion of this sub-band.

The local distortion of the Fe_A sublattice gives a preferential axis to the system—in this case along the y-direction (figures 1 and 3). The O atoms in the plane O_1–Fe–O_2 have moved outward, while the O_3 and O_4 atoms underwent diagonal inward relaxation but with slight twisting about the y axis (figure 1). Neutron-scattering studies at temperatures just above T_V suggest two possible condensing phonon modes Δ_4 and Δ_5 [35, 36]. Despite the small cell used in our model, the relaxation pattern of FeO_4 tetrahedra in E_{min} is similar to the Δ_4-mode, with the difference that in our results the O appear to have displacements with y-components and small twisting on two of them. A similar relaxation pattern has been observed in another theoretical study but they propose the Δ_5-mode as predominant above T_V [34].

With just two Fe_B and one Fe_4O_4 minicube per pc, any CO in E_{min} will produce the simple CO pattern originally proposed by Verwey [2]. This is evident in figure 3(c), where two ↓ electrons partially localize on the Fe_{B1} of every second (0 0 1) plane. This CO pattern is illustrated in figure 4(a). We note that a long Fe_B–O occurs in the plane of occupied Fe-d (y–z in figure 3), consistent with the JT effect.

3.2. 56-atom tetragonal model

In order to determine a more realistic CO pattern, full ionic relaxation (only internal coordinates) was also carried out in the $a/\sqrt{2} \times a/\sqrt{2} \times 2a$ tetragonal supercell (56 atoms). Different starting geometries led to two optimized structures. The $P1$ structure is just

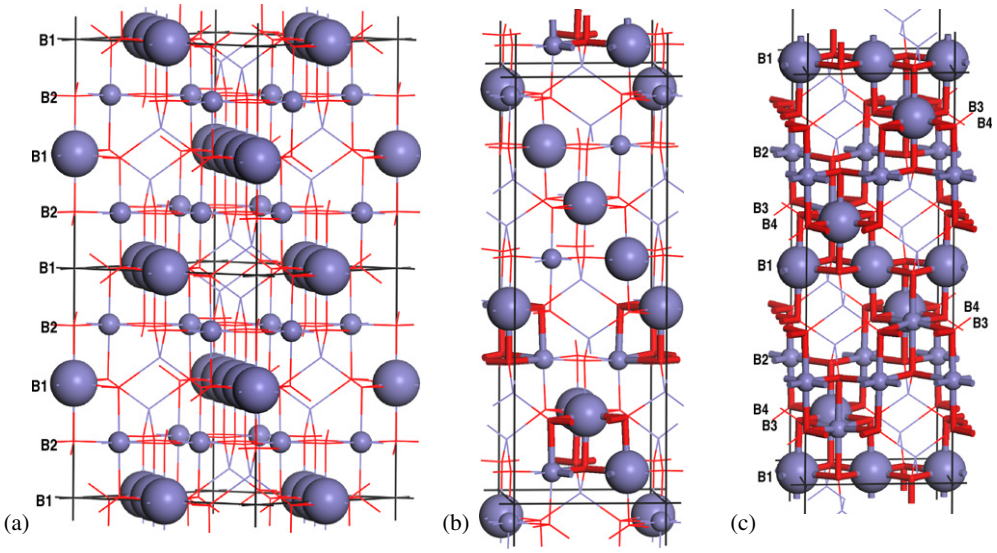

Figure 4. The CO pattern based on GGA + U Fe_B–O distances (table 1). (a) E_{min} ($C2/C$) showing CO that alternates in (0 0 1) layers in an $a\times a\times 2a$ cell. (b) $P1$ and (c) *Pmca*, both showing the $a/\sqrt{2}\times a/\sqrt{2}\times 2a$ cell. Red = O, blue = Fe (large balls = Fe_{B1}, small balls = Fe_{B2}, lines = Fe_A); thicker bonds indicate Fe_4O_4 minicubes that do not fulfil the Anderson criterion [21].

10 meV/fu more stable than E_{min} (table 1). The band structure of $P1$ is shown in figure 2(e) and shows a band gap of 0.31 eV, similar to E_{min}. The *Pmca* structure is another 16 meV/fu more stable, or 378 meV/fu lower in energy than the $Fd\bar{3}m$ structure E_C, slightly more than computed at an unrelaxed geometry [18].

The ions in the $P1$ structure adopt partial CO in a pattern that differs from the Verwey model. The electrons in the range 0.7 eV below E_F show mainly Fe-d character with a small O-p contribution and are partially localized on half of the Fe_B, agreeing in these respects with our results for the 14-atom cell. Unlike the symmetry imposed in [4, 17, 18], in this structure all 16Fe_B per cell are inequivalent. Averaging over the Fe_B–O distances for each Fe_B gives two clear sets of distances, correlating with the partial CO of the ↓ electrons near E_F (table 1). Around the sites where these electrons partially localize, the average Fe_B–O and magnetic moment have increased to ∼2.10 Å and 4.12 μ_B, respectively (like B1 in section 3.1), while around the remaining Fe_B sites, these distances and magnetic moment have decreased to ∼2.04 Å and 3.66 μ_B, respectively (B2). The distortions $\overline{\Delta r}(Fe_A)$, $\overline{\Delta r}(Fe_B)$ and $\overline{\Delta r}(O)$ are 0.04, 0.03 and 0.07 Å, respectively. Thus, the overall magnitude of Fe_A and O distortion in the 14-atom cell is reproduced in the 56-atom supercell, and the major difference is an additional distortion of the Fe_B sublattice in the latter. The coordinates of the $P1$ structure are given in supplementary data (available at stacks.iop.org/JPhysCM/18/10427). The CO pattern for $P1$ is shown in figure 4(b). Six out of the eight Fe_4O_4 minicubes in the cell contain equal numbers of Fe_{B1} and Fe_{B2} and so satisfy the Anderson criterion [21], while one minicube is electron-rich and one is electron-poor.

Optimization of the 56-atom cell within *Pmca* symmetry was found to give the lowest energy (by just 16 meV/fu). This reproduces correctly the pattern of O distortions about Fe_B that was determined by fitting to experiment within *Pmca* [4]. Indeed, computed Fe_B–O distances (table 1) are overestimated by just 0.01–0.05 Å relative to experiment, as is typical

of GGA, despite using an undeformed tetragonal cell. The pattern of partial CO (figure 4(c))—in particular, the predominant $d_{xz} \pm d_{yz}$ character at Fe^{2+}_{B1}-sites, is in agreement with previous unrelaxed monoclinic calculations using DFT + U [17, 18]. Two symmetry-distinct Fe_4O_4 minicubes are repeated within the cell and, as dictated by *Pmca* symmetry, one is electron-rich (formally $3Fe^{2+} + Fe^{3+}$) and one is electron-poor ($Fe^{2+} + 3Fe^{3+}$), so that the Anderson criterion is not fulfilled.

4. Discussion

GGA + U calculations of various systems with lower symmetry than the $Fd\bar{3}m$ phase of Fe_3O_4 are presented. All of these are found to have lower total energy than the $Fd\bar{3}m$ phase, and so they are candidate models for the low-temperature phase ($T < T_V$).

Our results suggest that the Verwey transition is a consequence of interplay between two different mechanisms, namely the electrostatic on-site Coulomb repulsion between electrons and the electron–phonon interactions (JT distortions). The on-site Coulomb repulsion among d electrons produces a $Fd\bar{3}m$ symmetry OO state (E_{LC}) or another OO state with broken-symmetry wavefunction (E_{LS}). In E_{LS}, the symmetry breaking OO of the electronic density on the top of the spin ↓ valence band is related to a dramatic change in the on-site Coulomb interaction energy $E_{\mathcal{U}}$ (see inset of figure 1). The energy differences between E_C, E_{LC} and E_{LS} disappear for less than a threshold $\mathcal{U}_c \approx 1.2$ eV, illustrating that CO solutions such as E_{LS} can only be found when an adequate + U correction is included, as stressed in earlier LDA + U work [18]. This demonstrates the importance of electron–electron repulsion in the Verwey transition, contrary to a previous assumption that this is a secondary effect [4]. Quantifying this, figure 1 shows that on-site Coulomb interactions allow the system to lower its energy by $E_C - E_{LS} \simeq 260$ meV/fu within the perfect cubic structure (figure 1), while the JT distortion involves a decrease in energy of another $E_{LS} - E(Pmca) \simeq 110$ meV/fu.

We find that the unstable states at cubic geometries become stable by coupling to an optical phonon. In the asymmetric case (E_{LS} to E_{min}) the phonon involves small distortions of O about Fe_B, reducing the anti-bonding interaction of O-p with ordered Fe-d orbitals, and so this is an example of the JT effect. Distortion is strongest on half of the Fe_B where partial localization of Fe-d has occurred (i.e. B1 sites). This leads to a non-cubic pattern of partial CO and the opening of a minority spin band gap. This confirms the prediction of Yanase *et al* based on the cubic band structure, that preferential occupation of some Fe_B will open a band gap [37]. Although the CO pattern is more complex in the actual Cc structure, we suggest that the same mechanism underlies the actual MIT in Fe_3O_4.

E_{LC} shows symmetric OO and symmetric relaxation of O atoms, which does not open a band gap. This illustrates that OO alone is not a sufficient condition for the MIT below T_V. In E_{LC}, the limited number of empty states just above E_F followed by a gap of ∼0.3 eV (figure 2(b)) are consistent with Fe_3O_4 appearing like a semiconductor, i.e. $d\rho/dT < 0$ (with ρ being the resistivity) as experiments reveal for $T_V < T < 300$ K [38].

We have thus determined the conditions required for band-gap opening. However our calculated value for the band gap (0.33 eV) is fitted by varying the $\mathcal{U}$ parameter. Previous studies using inter-site LDA + U [30] predict a CO state with a band gap of 0.35 eV and no ionic deformations. A 0.35 eV band gap is also found using the self-interaction corrected local spin-density approximation [39], based on Verwey CO within the cubic structure, but a lower energy solution with no band gap is also found.

In our approach, the electrons at the top of the ↓ valence band have some degree of delocalization—as demonstrated by the appreciable band dispersion just below E_F (figure 2) and by the partial electronic localization in real space with some charge transfer to O atoms

(figure 3). However, the extent of localization or CO onto Fe_{B1} is likely to be sensitive to the value of the fitted parameter $\mathcal{U}$, and so we do not attempt to quantify it.

We have considered three possible CO patterns in the tetragonal cell (figure 4). The *Pmca* structure, with all Fe_4O_4 minicubes violating the Anderson criterion, is computed to be more stable than the Verwey ordering of $C2/C$, where all minicubes fulfil this criterion [21]. Although the energy differences are slight (26 meV/fu), it is clear that pure electrostatics (underlying the Anderson criterion) is not the main factor determining the stability of CO patterns. Specific geometry-dependent interaction between ordered Fe and O orbitals (i.e the JT effect) appears to be more important.

We have not computed the full $\sqrt{2}a\times\sqrt{2}a\times 2a$ Cc cell of 224 atoms. Other than the Verwey model, there are nine models for CO in the Cc cell that conform to the Anderson criterion [14]. A plausible non-Anderson model has also been proposed featuring various orientations of the mixed layers of the *Pmca* pattern [12]. We note that the Cc cell features 16 inequivalent Fe_B [14], in common with our computed $P1$ structure, so that 2×2 expansion of a structure like $P1$ under Cc symmetry operations would yield another candidate Cc structure.

By deliberately studying a small 14-atom model in detail, we have been able to show that the necessary conditions for band-gap opening in low-temperature Fe_3O_4 are (i) on-site Fe-d electron–electron repulsion and (ii) JT distortion of O about Fe_B. Distortion of Fe_A is a secondary effect, responding to O distortion. It suffices to consider a single Fe_4O_4 minicube; similar distortions of the O sublattice are computed to occur in a larger cell of eight inequivalent minicubes. Even after JT distortion, CO on the cubic Fe_B sublattice is frustrated and this leads to further secondary effects: distortion of Fe_B, cell-doubling along [0 0 1] and monoclinicity, finally producing the low-temperature phase. None of these are necessary conditions for band-gap opening in this system, but rather consequences of the CO that accompanies it. We estimate the energy gained in the secondary relaxations of the phase change to be an order of magnitude smaller than that due to the JT-driven band-gap opening alone.

5. Conclusion

In conclusion, the interplay between on-site Coulomb repulsions on Fe_B (undergoing a dramatic decrease in the $E_{\mathcal{U}}$ energy) and electron–phonon interactions (involving a JT distortion of O atoms about Fe_B) are essential in opening a band gap in the low-temperature phase of Fe_3O_4. The band-gap opening is consistent with the drop in resistivity observed during the Verwey transition. The resulting electronic structure shows the persistent itinerant nature of the electrons near E_F with a partial charge localization onto half of the Fe_B and a slight charge transfer to the O atoms. Some evidence is supplied that the phase transition from cubic to monoclinic is due to the frustrated charge-ordering pattern on the Fe_B sublattice.

Acknowledgments

We thank R M Nieminen, A Amann and S Fahy for fruitful discussions. This work was funded by the Irish Research Council for Science, Engineering and Technology.

References

[1] Eereinstein W, Palstra T T M, Saxena S S and Hibma T 2002 *Phys. Rev. Lett.* **88** 247204
[2] Verwey E J W 1939 *Nature* **144** 327
[3] Iizumi M, Koetzle T F, Shirane G, Chikazumi S, Matsui M and Todo S 1982 *Acta Crystallogr.* B **38** 2121
[4] Wright J P, Attfield J P and Radaelli P G 2001 *Phys. Rev. Lett.* **87** 266401

[5] Park J-H, Tjeng L H, Allen J W, Metcalf P and Chen C T 1997 *Phys. Rev.* B **55** 12813
[6] Chainani A, Yokoya T, Morimoto T, Takahashi T and Todo S 1995 *Phys. Rev.* B **51** 17976
[7] Park S K, Ishikawa T and Tokura Y 1998 *Phys. Rev.* B **58** 3717
[8] Coey M 2004 *Nature* **430** 155
[9] Walz F 2002 *J. Phys.: Condens. Matter* **14** R285
[10] García J and Subías G 2004 *J. Phys.: Condens. Matter* **16** R145
[11] Goff R J, Wright J P, Attfield J P and Radaelli P G 2005 *J. Phys.: Condens. Matter* **17** 7633
[12] Nazarenko E, Lorenzo J E, Joly Y, Hodeau J L, Mannix D and Marin C 2006 *Phys. Rev. Lett.* **97** 056403
[13] Rudee M L, Smith D J and Margulies D T 1999 *Phys. Rev.* B **59** R11633
[14] Zuo J M, Spence J C H and Petuskey W 1990 *Phys. Rev.* B **42** 8451
[15] Siratori K, Ishii Y, Morii Y, Funahashi S, Todo S and Yanase A 1998 *J. Phys. Soc. Japan* **67** 2818
[16] García J, Subıas G, Proietti M G, Blasco J, Renevier H, Hodeau J L and Joly Y 2000 *Phys. Rev.* B **63** 054110
[17] Leonov I, Yaresko A N, Antonov V N, Korotin M A and Anisimov V I 2004 *Phys. Rev. Lett.* **93** 146404
[18] Guo G Y, Jeng H-T and Huang D J 2004 *Phys. Rev. Lett.* **93** 156403
[19] Seo H, Ogata M and Fukuyama H 2002 *Phys. Rev.* B **65** 085107
[20] Subías G, García J and Blasco J 2005 *Phys. Rev.* B **71** 155103
[21] Anderson P W 1956 *Phys. Rev.* **102** 1008
[22] Kresse G and Furthmüller J 1996 *Comput. Mater. Sci.* **6** 15
[23] Kresse G and Furthmüller J 1996 *Phys. Rev.* B **54** 11169
[24] Perdew J P, Chevary J A, Vosko S H, Jackson K A, Pederson M R, Singh D J and Fiolhais C 1992 *Phys. Rev.* B **46** 6671
[25] Dudarev S L, Botton G A, Savrasov S Y, Humphreys C J and Sutton A P 1998 *Phys. Rev.* B **57** 1505
[26] Kresse G and Joubert J 1999 *Phys. Rev.* B **59** 1758
[27] Okudera H, Kihara K and Matsumoto T 1996 *Acta Crystallogr.* B **52** 450
[28] Aragon R 1992 *Phys. Rev.* B **46** 5328
[29] Finger L W, Hazen R M and Hofmeister A M 1986 *Phys. Chem. Mineral.* **13** 215
[30] Anisimov V I, Elfimov I S, Hamada N and Terakura K 1996 *Phys. Rev.* B **54** 4387
[31] Antonov V N, Harmon B N, Antropov V P, Perlov A Ya and Yaresko A N 2001 *Phys. Rev.* B **64** 134410
[32] Huang D J, Chang C F, Jeng H-T, Guo G Y, Lin H-J, Wu W B, Ku H C, Fujimori A, Takahashi Y and Chen C T 2004 *Phys. Rev. Lett.* **93** 077204
[33] Zhang Z and Satpathy S 1991 *Phys. Rev.* B **44** 13319
[34] Seo H, Ogata M and Fukuyama H 2002 *Phys. Rev.* B **65** 085107
[35] Fujii Y, Shirane G and Yamada Y 1975 *Phys. Rev.* B **11** 2036
[36] Yamada Y, Wakabayashi N and Nicklow R M 1980 *Phys. Rev.* B **21** 4642
[37] Yanase A and Hamada N 1999 *J. Phys. Soc. Japan* **68** 1607
[38] Miles P A, Westphal W B and Hippel V A 1957 *Rev. Mod. Phys.* **29** 279
[39] Szotek Z, Temmerman W M, Svane A, Petit L, Stocks G M and Winter H 2003 *Phys. Rev.* B **68** 054415